Disconnecting the Golgi ribbon from the centrosome prevents directional cell migration and ciliogenesis

Lidia Hurtado,[1] Cristina Caballero,[1] Maria P. Gavilan,[1] Jesus Cardenas,[1] Michel Bornens,[2] and Rosa M. Rios[1]

[1]Departamento de Señalización Celular, Centro Andaluz de Biología Molecular y Medicina Regenerativa–Consejo Superior de Investigaciones Científicas, 41092-Seville, Spain
[2]Unité Mixte de Recherche 144, Centre National de la Recherche Scientifique–Institut Curie, 75252 Paris, Cedex 05, France

Mammalian cells exhibit a frequent pericentrosomal Golgi ribbon organization. In this paper, we show that two AKAP450 N-terminal fragments, both containing the Golgi-binding GM130-interacting domain of AKAP450, dissociated endogenous AKAP450 from the Golgi and inhibited microtubule (MT) nucleation at the Golgi without interfering with centrosomal activity. These two fragments had, however, strikingly different effects on both Golgi apparatus (GA) integrity and positioning, whereas the short fragment induced GA circularization and ribbon fragmentation, the large construct that encompasses an additional p150*glued*/MT-binding domain induced separation of the Golgi ribbon from the centrosome. These distinct phenotypes arose by specific interference of each fragment with either Golgi-dependent or centrosome-dependent stages of Golgi assembly. We could thus demonstrate that breaking the polarity axis by perturbing GA positioning has a more dramatic effect on directional cell migration than disrupting the Golgi ribbon. Both features, however, were required for ciliogenesis. We thus identified AKAP450 as a key determinant of pericentrosomal Golgi ribbon integrity, positioning, and function in mammalian cells.

Introduction

In mammalian cells, the Golgi apparatus (GA) is a single-copy organelle localized around the centrosome (CTR). This organization depends on microtubules (MTs) and the MT motor dynein. In the absence of MTs or dynein activity, the Golgi ribbon fragments and GA stacks appear scattered throughout the cytoplasm (Brownhill et al., 2009). Depletion of peripheral GA proteins also affects GA integrity and position, indicating that they contribute to maintain this organization (Diao et al., 2003; Rios et al., 2004; Yadav et al., 2009). The GA and the CTR are also functionally linked (Sütterlin and Colanzi, 2010). The Golgi proteins GM130, Cdc42, and Tuba constitute a complex that regulates CTR morphology and function during interphase (Kodani and Sütterlin, 2008; Kodani et al., 2009), whereas GRASP65 (Sütterlin et al., 2005), Tankyrase (Chang et al., 2005), or the phosphatase Sac1 (Liu et al., 2008) is required for correct mitotic spindle formation. Conversely, several centrosomal proteins, including AKAP450 (Takahashi et al., 1999), CEP350 (Hoppeler-Lebel et al., 2007), and CDK5Rap2 (Barr et al., 2010), are associated with the GA.

It is known that pericentrosomal Golgi ribbon organization is not critical for protein modification or global secretion, which is not significantly affected when the ribbon is severed into individual stacks (Thyberg and Moskalewski, 1999). Recent data suggest a role for the ribbon in directed secretion and migration and in cell cycle progression. Cells lacking GMAP210 or Golgin-160, in which the Golgi ribbon was fragmented but the MT network remained apparently intact, failed to secrete proteins in a directional manner and to efficiently polarize and migrate in response to wounding (Yadav et al., 2009). Because depletion of these proteins caused the loss of both integrity and position of the GA, the question of whether GA pericentrosomal position, itself, is required for directional secretion and migration could not be addressed. On the other hand, maintaining an intact pericentrosomal Golgi ribbon during G2/M transition was shown to prevent entry into mitosis. Breaking the Golgi ribbon into

L. Hurtado, C. Caballero, and M.P. Gavilan contributed equally to this paper.

Correspondence to Rosa M. Rios: rosa.rios@cabimer.es

Abbreviations used in this paper: CLASP, cytoplasmic linker protein–associated protein; CTR, centrosome; ERES, endoplasmic reticulum exit sites; GA, Golgi apparatus; GT, galactosyltransferase; HSD, honestly significant difference; IF, immunofluorescence; IP, immunoprecipitation; MT, microtubule; NPY, neuropeptide Y; NZ, nocodazole; PM, plasma membrane; WB, Western blotting.

The Rockefeller University Press $30.00
J. Cell Biol. Vol. 193 No. 5 917–933
www.jcb.org/cgi/doi/10.1083/jcb.201011014

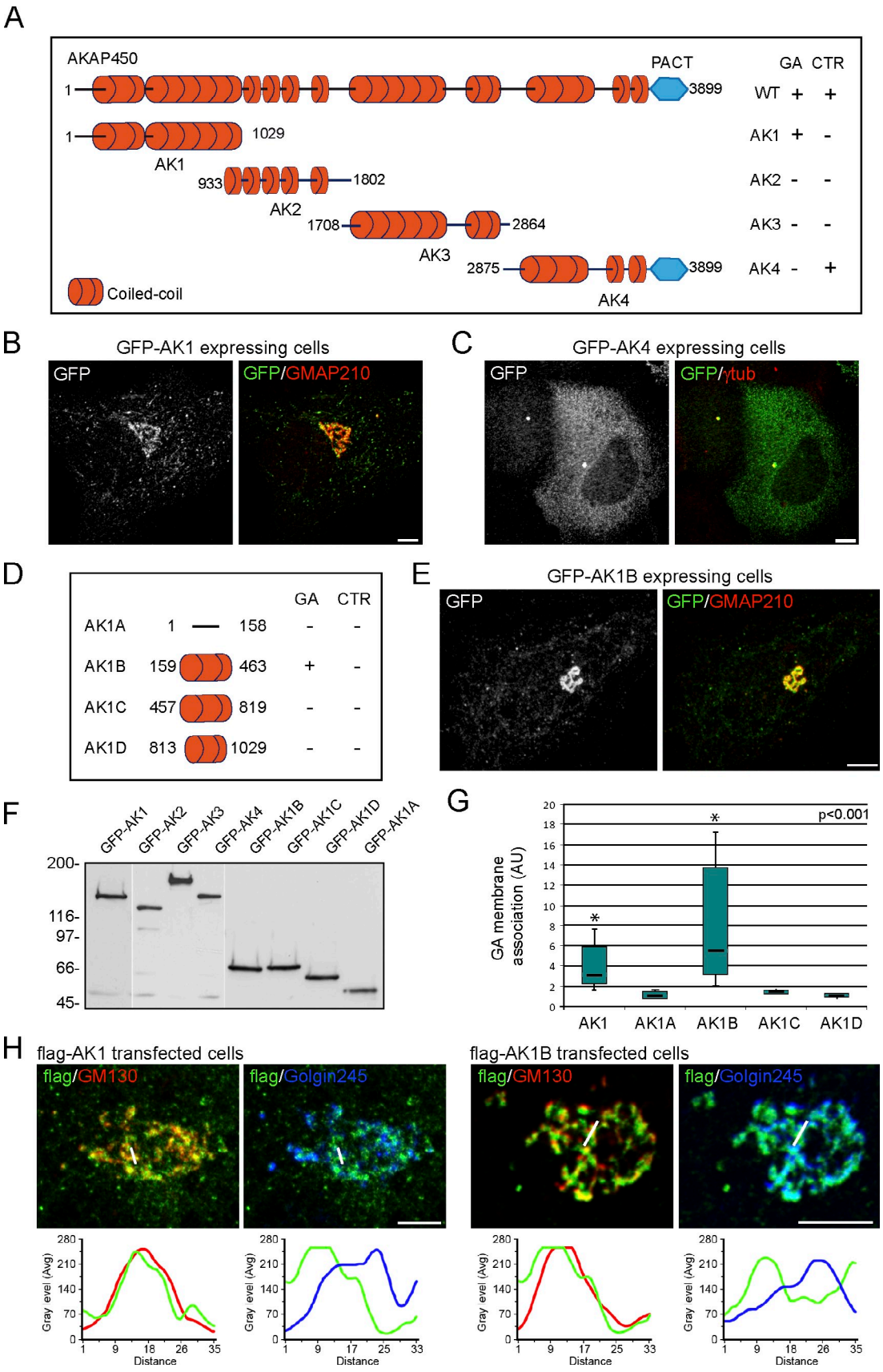

Figure 1. **Identification of the AKAP450 cis-Golgi–targeting domain by serial truncations.** (A and D) Schematic representation of the AKAP450-truncated mutants used in this study. (right) A summary of the subcellular localization of each fragment. (B, C, and E) GFP-AK1 (B)–, GFP-AK4 (C)–, or GFP-AK1B (E)–expressing cells were labeled for GMAP210 (B and E) or γ-tubulin (C). Merged images are shown on the right. (F) WB of RPE-1 cells expressing AKAP450-truncated

isolated stacks, which normally occurs during G2, allowed the cells to progress into mitosis (Sütterlin et al., 2002).

Recently, the ability of the GA to nucleate MTs has been demonstrated, and the molecular machinery has been partly identified (Efimov et al., 2007; Rivero et al., 2009). This machinery includes (a) the γ-tubulin–interacting protein AKAP450 that is recruited to cis-GA membranes via GM130, (b) the dynein–dynactin activity, and (c) the MT plus end–binding proteins, cytoplasmic linker protein–associated proteins (CLASPs), that are anchored to the trans-GA membranes via GCC185. The function of GA-nucleated MTs has also been investigated (Miller et al., 2009). After mitosis or during nocodazole (NZ) recovery, the subset of Golgi-nucleated MTs is required for the assembly of GA fragments into larger elements in the cell periphery (G stage). In a second stage, centrosomal MTs provided the tracks along which GA elements are transported to the cell center and then tangentially connected into a ribbon (C stage). When MT nucleation at the GA is specifically inhibited, only the CTR-based MT array persists and a fragmented GA collapses around the CTR. Thus, GA-based MTs are responsible for Golgi ribbon integrity and extended morphology. Finally, GA-nucleated MTs reinforce the asymmetry of the MT network that is essential for cell polarization, a prerequisite for directional cell migration (Vinogradova et al., 2009). In spite of these findings, many questions concerning the organization and the physiological significance of the GA/CTR association remain unanswered. Until now, the lack of experimental conditions permitting the separation of an intact Golgi ribbon from the CTR made it difficult to evaluate their individual role in secretion, cell polarity, and migration.

In this work, we have undertaken a systematic truncation analysis to identify the GA-targeting domain of the CTR/GA-associated protein AKAP450. A GA-binding GM130-interacting domain has been mapped at the first N-terminal 300-aa coiled-coil stretch of the protein. Expression of this domain dissociated AKAP450 from GA, inhibited MT nucleation at the GA, and resulted in a fragmented GA collapsed around the CTR. Strikingly, the expression of a larger N-terminal fragment that also includes a MT-binding p150*glued*-interacting domain preserved the integrity of the Golgi ribbon but not its pericentrosomal localization. The effects of expression of these truncated mutants on GA biogenesis, secretion, polarization, migration, and primary cilium formation have been analyzed.

Results

An N-terminal sequence mediates recruitment of AKAP450 to Golgi membranes

To characterize the regions of AKAP450 required for its localization to the GA, we divided the full-length protein in four large fragments (AK1–AK4), all of them containing long coiled-coil regions (Fig. 1 A). Truncated mutants were fused to different tags and transfected in RPE-1 cells. Only the AK1 fragment corresponding to the N terminus of the protein was targeted to the GA as revealed by double labeling for GMAP210. Some punctuate and fibrillar structures were also observed throughout the cytoplasm (Fig. 1 B). AK2 and AK3 fragments were cytoplasmic (Fig. S1 A), whereas the C-terminal fragment AK4 that contains the pericentrin-AKAP450 centrosomal targeting domain (Gillingham and Munro, 2000) localized to the CTR as expected (Fig. 1 C). Similar distribution was observed in MCF10A cells (Fig. S1 B).

A series of additional truncations of the AKAP450 N terminus, AK1A to AK1D (Fig. 1 D), revealed that the GA-binding motif is contained in the AK1B mutant corresponding to aa 159–463, a sequence that exactly encompasses the first coiled-coil stretch of the protein (Fig. 1 E). Remarkably, the AK1B labeling was strictly congruent with that of the cis-GA marker GMAP210 (Fig. 1 E and see Fig. S1 for the other mutants). We checked that all AKAP450 mutants were properly expressed in these cells (Fig. 1 F). Finally, the level of GA recruitment for all N-terminal constructs was quantified and normalized to cytoplasm intensity (Fig. 1 G). Using different GA compartment markers, confocal microscopy and fluorescence intensity profile analysis revealed a higher degree of colocalization of both AK1 and AK1B mutants with the cis-GA marker GM130 than with the trans-GA marker Golgin-245 (Fig. 1 H). Thus, the distribution pattern of AKAP450 N-terminal mutants inside the GA is similar to that of the endogenous protein (Rivero et al., 2009). Furthermore, AK1 and AK1B association with membranes was maintained when MT or GA dynamics was perturbed by drug treatments (Fig. S2).

Both AK1 and AK1B expressions trigger AKAP450 network disassembly but differently affect GA positioning and morphology

The expression of both AK1 and AK1B domains completely disassembled the GA-associated AKAP450 network without affecting the centrosomal fraction (Fig. 2, A and E). The large N-terminal AK1 mutant induced a dramatic change in the position of the GA relative to the CTR (Fig. 2 A). The GA appeared either as a single structure or fragmented in two or three large elements that remained together and connected by membrane tubules away from the CTR. Fig. 2 B shows the GA surrounding the CTR in a nontransfected cell. No significant perturbation of the CTR-nucleated MT network was observed in transfected cells (Fig. 2 C). AK1-containing cytoplasmic punctate or fibrillar structures aligned with MTs were also observed (Fig. 2 D). These structures became randomly distributed when MTs were depolymerized (see Fig. 4 and Fig. S2), suggesting that the

mutants used in this study. Molecular masses are given in kilodaltons. (G) Box and whisker plot showing quantification of GA recruitment for each N-terminal mutant. Top and bottom ends of the boxes represent 75th and 25th percentiles, and whiskers represent 90th and 10th percentiles. The median is depicted with a solid line. Asterisks denote significant statistical differences ($P < 0.001$; Tukey honestly significant difference [HSD]). $n = 30$ cells scored per mutant from three independent experiments. AU, arbitrary unit. (H) Merged images of cells expressing flag-AK1 or flag-AK1B double labeled for flag and either GM130 or Golgin-245. Fluorescence intensity profiles corresponding to lines drawn in each image from the top gallery are shown on the bottom. PACT, pericentrin-AKAP450 centrosomal targeting domain; WT, wild type. Bars, 5 µm.

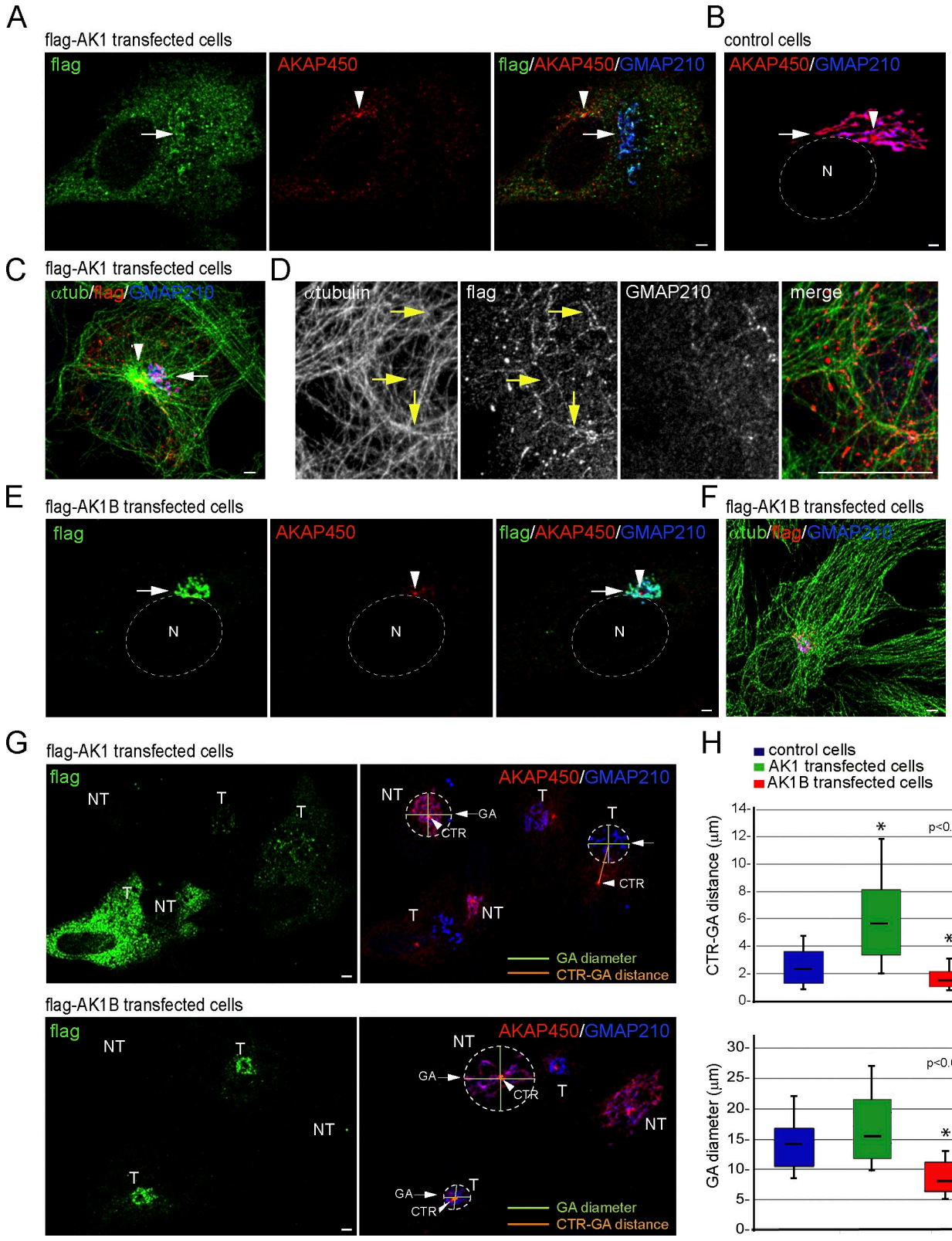

Figure 2. **AK1 and AK1B fragments differentially affect GA positioning and morphology.** (A) RPE-1 cells expressing the flag-AK1 fragment were triple labeled for flag, AKAP450, and GMAP210. Single labelings and the merge are shown. White arrows and arrowheads indicate the GA and the CTR, respectively. In B, a nontransfected cell is shown for comparison. N, nucleus. (C) Merged image of a flag-AK1–transfected cell stained for flag, α-tubulin, and GMAP210 to visualize the MT network. (D) High magnification images of a flag-AK1–transfected cell triple labeled as in C. Single labelings in black and white and the merge are shown. Yellow arrows indicate the alignment of AK1B-containing structures with MTs. (E and F) Merged images of flag-AK1B–expressing cells triple labeled as in A or C, respectively. (G) Low magnification images of flag-AK1 (top)– and flag-AK1B (bottom)–transfected cells triple labeled for flag, AKAP450, and GMAP210. Single labelings for flag are shown on the left to identify transfected cells (T). (right) Schematic of the measurement of CTR–GA distance and GA diameter over the corresponding AKAP450 and GMAP210 merged images. A straight line connecting the center of the

AKAP450 N-terminal domain associates with MTs. In contrast, AK1B expression resulted in the collapse of the GA around the CTR (Fig. 2 E); the GA changed from an extended ribbon to a circular morphology around the CTR (compare Fig. 2, E and B). MT aster also appeared to be more focused (Fig. 2 F). These effects on GA were reminiscent of that induced by AKAP450 siRNA (Fig. S4 B), suggesting that this fragment behaves as a dominant-negative mutant. It should be noted that AK2, AK3, and AK4 fragment expression, all of them consisting of long coiled-coil domains, did not affect GA morphology or positioning regardless of their expression levels (Fig. S1), thus confirming the specificity of AK1- and AK1B-induced effects on GA.

To further characterize these phenotypes, we measured the distance between the CTR and the center of a circumference circumscribing the GA in nontransfected, AK1-transfected, or AK1B-transfected cells as represented in Fig. 2 G (top). The diameter of these circumferences was also determined as an index of GA circularity (Fig. 2 G, bottom). The mean distance between the GA and the CTR was ∼2.4 µm in nontransfected cells, 5.5 µm in AK1-transfected cells, and only 1.5 µm in AK1B-transfected RPE-1 cells. Remarkably, in a few AK1-transfected cells, the distance from the GA to the CTR was >15 µm. Regarding the Golgi circularity index, slight differences were detected between nontransfected and AK1-transfected cells, whereas the diameter of the GA in AK1B-expressing cells was reduced by >40%. Thus, AK1-expressing cells exhibited an almost normal-sized GA located far from the CTR (the distance increased >2.3 times), whereas AK1B-expressing cells contain a circular GA condensed around the CTR (both GA size and the distance to the CTR were reduced by 40%).

To exclude that observed effects on Golgi position and morphology were dependent on cell heterogeneity, we normalized the GA–CTR complex of control, GFP-AK1–, and GFP-AK1B–transfected cells by plating them on Y-shaped micropatterned coverslips (Fig. S3). Micropatterned cells fully confirmed the phenotype observed in cells grown under standard conditions.

Both AK1 and AK1B interact with GM130, but only AK1 binds p150*glued* and MTs

Endogenous GM130 was able to pull down both GFP-AK1 and GFP-AK1B (Fig. 3 A). A reciprocal coimmunoprecipitation (IP; co-IP) experiment showed an interaction between GFP-AK1B and YFP-GM130 in double-transfected cells (Fig. 3 B). No interaction was detected with the other partial constructs that do not target the GA, namely GFP-AK2 (Fig. 3 A), GFP-AK3, or GFP-AK4 fragments (Fig. S4 A). These experiments demonstrate a specific interaction of both AK1 and AK1B with GM130.

To further investigate whether the AK1B–GM130 interaction mediates GA targeting of AKAP450 in vivo, we analyzed AK1B capacity to bind GA membranes in the absence of GM130 (Fig. 3 C). RPE-1 cells were depleted of GM130 by siRNA and then transfected with the flag-tagged version of AK1B. In addition, cells were treated with NZ to induce fragmentation and dispersion of the GA into Golgi ministacks. In NZ-treated flag-AK1B–transfected cells, the truncated protein remained partly associated with GA ministacks (Fig. 3 C, left, high magnifications). In contrast, GM130 depletion promoted a striking loss of AK1B from GA elements (Fig. 3 C, right, high magnifications), confirming that the association of AKAP450 to the GA involves GM130 and aa 159–463 of AKAP450. We further demonstrated that AK1 and AK1B fragments were able to dimerize (Fig. 3 D), a feature that could favor interaction with GM130. Co-IP experiments from cells expressing both GFP- and flag-tagged versions of AK1 and AK1B demonstrated that it is the case.

Finally, we investigated the MT-binding properties of both N-terminal fragments. The γ-tubulin small complex binding site of AKAP450 has been mapped by others in a region roughly corresponding to the AK1 domain (Takahashi et al., 2002). However, we were unable to detect any interaction of the AK1 fragment with either GCP3 or γ-tubulin even after extensive co-IP analysis. Instead, we found that this domain interacted with p150*glued* (Fig. 3 E) and partly cosedimented with taxol-stabilized MTs (Fig. 3 F), in agreement with our immunofluorescence (IF) data. The small AK1B fragment did not bind either p150*glued* or MTs under similar conditions (Fig. 3, E and F). We conclude that the large AK1 fragment is a dimer containing GA and MT binding sites, whereas the short AK1B dimer only contains the GA binding site. A summary of the properties of AK1 and AK1B fragments is shown in Fig. 3 G.

Both AK1 and AK1B expression inhibits MT nucleation at the GA

We then investigated whether expression of AKAP450 N-terminal fragments that dissociated AKAP450 from the GA also prevented MT nucleation (Fig. 4). First, cells expressing AK1 were cold treated to depolymerize MTs without affecting GA integrity and position and then rewarmed as indicated (Fig. 4 A). MT nucleation activity at the CTR was normal at both time points. In contrast, the GA had lost the ability to nucleate MTs (Fig. 4 A). Similar results were obtained from NZ recovery experiments in AK1B-expressing cells. After NZ removal, no MTs were seen growing from the GA elements, contrary to what occurs in nontransfected cells (Fig. 4 B, right). MT nucleation at the CTR was unaffected, and a radial array was eventually formed. These results confirm our previous data based on siRNA indicating that the AKAP450–GM130 interaction in the cis-GA surface is essential for MT nucleation at the GA.

AKAP450 ensures Golgi ribbon continuity

A puzzling result was that both AK1 and AK1B fragments inhibited MT nucleation at the GA, yet their effects on GA morphology and positioning were strikingly different. GA-nucleated

circumferences circumscribing the GA and the CTR was measured to calculate the CTR–GA distance. GA diameter was used as an index of GA circularity. NT, not transfected. (H) Graphs showing quantification of the CTR–GA distance (top) and Golgi circularity index (bottom; $n = 160$ for each condition from three independent experiments). Data are presented in the same box and whisker format as in Fig 1 with the median marked as a solid line (*, $P < 0.001$; Tukey HSD). Top and bottom ends of the boxes represent 75th and 25th percentiles, and whiskers represent 90th and 10th percentiles. Bars, 2.5 µm.

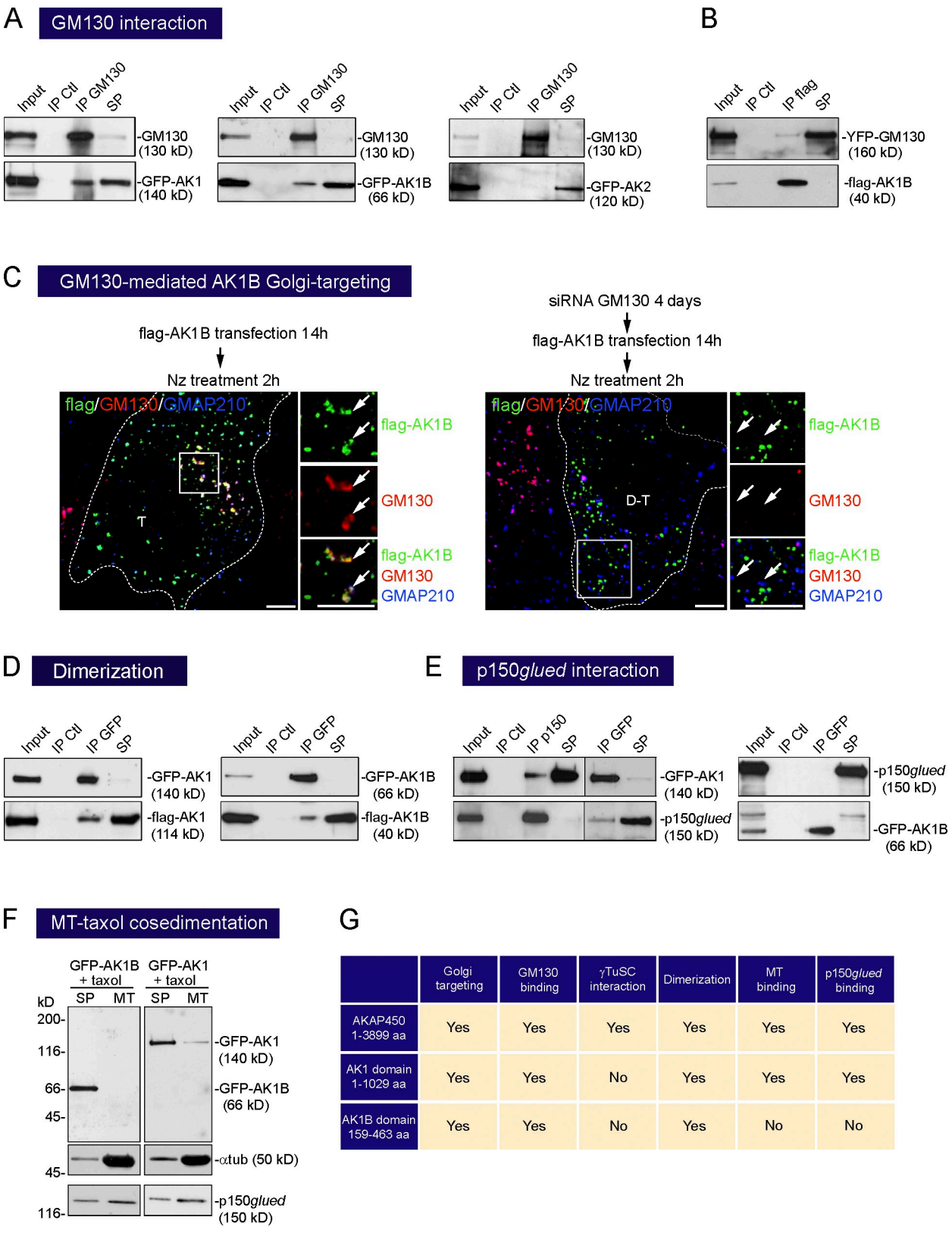

	Golgi targeting	GM130 binding	γTuSC interaction	Dimerization	MT binding	p150*glued* binding
AKAP450 1-3899 aa	Yes	Yes	Yes	Yes	Yes	Yes
AK1 domain 1-1029 aa	Yes	Yes	No	Yes	Yes	Yes
AK1B domain 159-463 aa	Yes	Yes	No	Yes	No	No

Figure 3. **Both AK1 and AK1B contain the GA-binding GM130-interacting domain, but only AK1 binds MTs.** (A) GFP-AK1–, GFP-AK1B–, and GFP-AK2–expressing cell extracts were immunoprecipitated with the anti-GM130 antibody, and blots were revealed for GM130 and GFP. Ctl, control; SP, supernatant. (B) Co-IP from flag-AK1B and YFP-GM130 double-transfected cell extracts using an anti-flag antibody. Blots were revealed for flag and GM130. (C) Control (left) or GM130-depleted (right) cells were transfected with the flag-AK1B construct and then NZ treated to fragment the GA into stacks. Labelings were for flag, GM130, and GMAP210 as indicated. Merged images are shown. Enlarged boxes on the right show single labelings or merges corresponding to outlined areas. T, transfected; D, depleted. Arrows indicate GA ministacks. Bars, 5 µm. (D) Cells coexpressing GFP- and flag-tagged versions of AK1 (left) or AK1B (right) were immunoprecipitated with an anti-GFP antibody, and blots were revealed for GFP and flag. (E) GFP-AK1–transfected cell

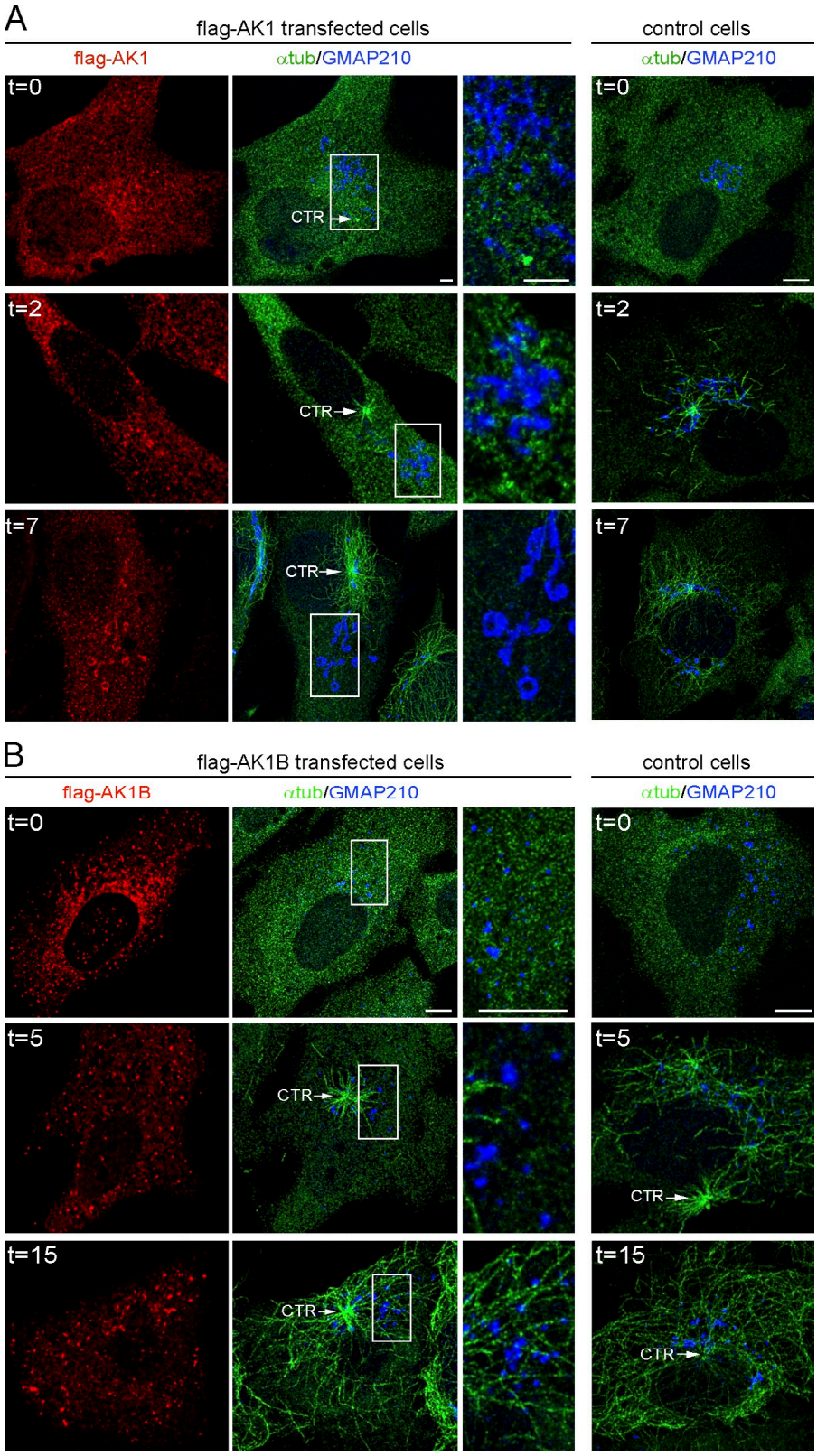

Figure 4. **Both AK1 and AK1B expression inhibits MT nucleation at the GA.** (A) Control or flag-AK1–transfected cells incubated on ice for 40 min to depolymerize MTs and rewarmed at the indicated times were triple stained for flag, α-tubulin (αtub), and GMAP210. Single labelings for flag are shown on the left, and the corresponding merged images for α-tubulin and GMAP210 are shown in the middle with enlarged boxes on the right. MT repolymerization in control cells at the same time points (minutes) is shown on the right for comparison. (B) Identical experiments were performed in flag-AK1B–transfected cells, but MTs were depolymerized by NZ treatment. At the indicated times after washout, cells were triple stained for flag, α-tubulin, and GMAP210. NZ recovery in control cells at the same time points is shown on the right for comparison. Bars, 2.5 μm.

extracts were immunoprecipitated either with anti-p150*glued* or anti-GFP antibodies (left). IPs were then tested for the presence of GFP-AK1 or p150*glued*. (right) A similar anti-GFP IP from GFP-AK1B–expressing cells is shown. Black lines separate parts from different gels. (F) MTs were polymerized from RPE-1 cell lysates expressing GFP-AK1 or GFP-AK1B in the presence of exogenous tubulin and taxol. After centrifugation through a sucrose cushion, supernatants (SP) and pellets (MT) were analyzed by WB for GFP, α-tubulin, and p150*glued* as a positive control. (G) A summary of properties of AKAP450 and the N-terminal AK1 and AK1B fragments. αtub, α-tubulin; γTuSC, γ-tubulin small complex.

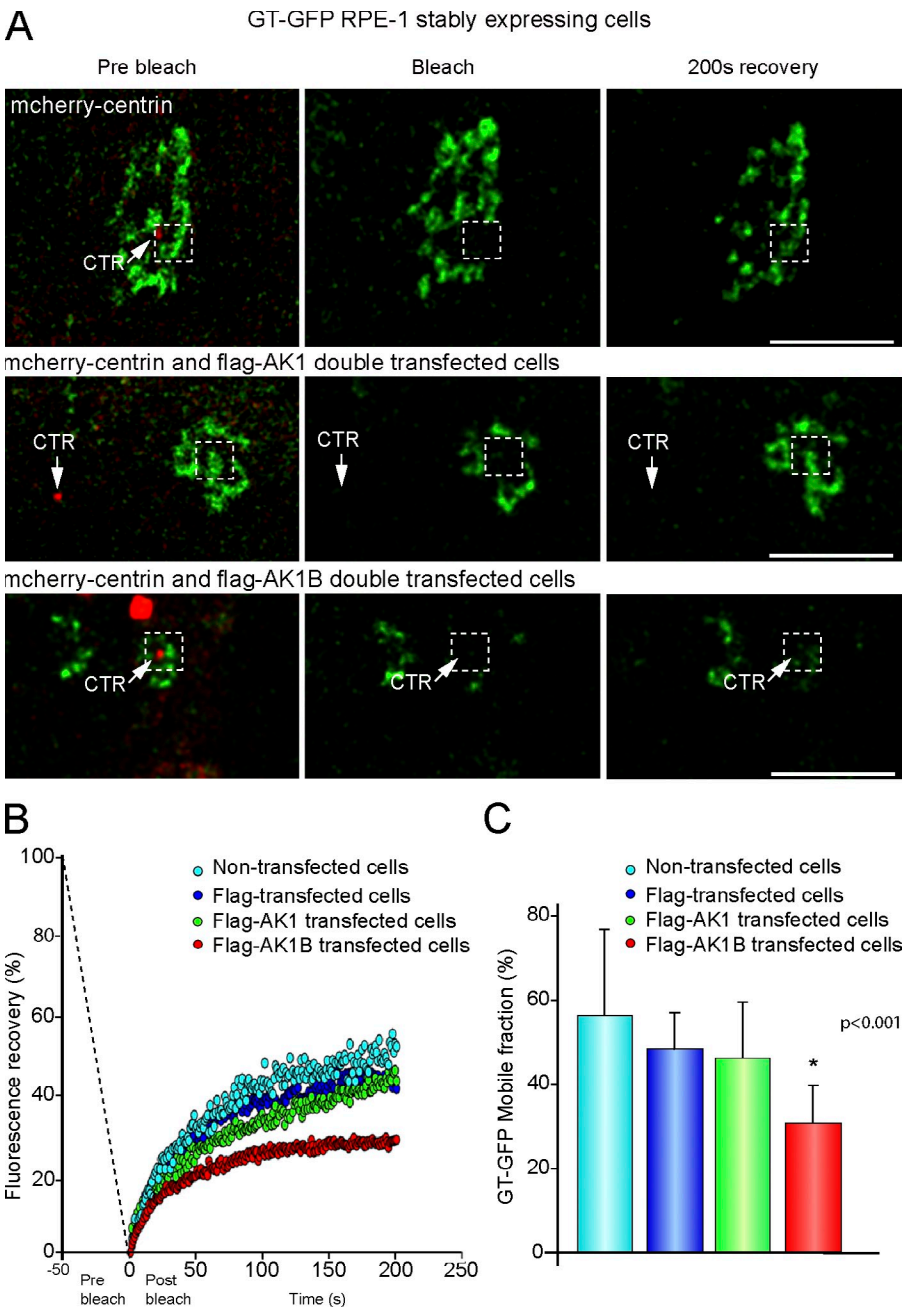

Figure 5. **The GA of AK1B-transfected cells exhibits diminished GT mobility, whereas it is not perturbed in AK1-transfected cells.** (A) FRAP experiments were performed in RPE-1 GT-GFP–expressing cells transfected with mCherry-centrin (top row) or cotransfected with mCherry-centrin and either flag-AK1 (middle row) or flag-AK1B (bottom row). (left) Images of selected cells are shown before bleaching (prebleach) with CTR in red and the GA in green. Video frames of the same cells 0 s after bleaching (middle images) and 200 s after bleaching (right images) are shown. Bleached regions are indicated by white squares. (B) Graph showing the percentage of fluorescence recovery intensity for nontransfected, flag-transfected, flag-AK1–, and flag-AK1B–transfected cells. n = 30 for each condition from five independent experiments. (C) Bar graph shows the percentage of GT-GFP mobile fraction under each condition for the same cells (*, $P < 0.001$; Holm-Sidak). Error bars indicate standard deviations. Bars, 5 µm.

MTs have been proposed to be required for tangential Golgi stack linking within the Golgi ribbon. To test the continuity of the GA in cells expressing AKAP450-truncated mutants, we performed FRAP experiments in a RPE-1 cell line stably expressing the galactosyltransferase (GT) membrane fragment GT-GFP (Fig. 5). To identify transfected cells and to localize CTRs, GT-GFP cells were transiently transfected with an mCherry-centrin construct or cotransfected with mCherry-centrin and either flag-AK1 or flag-AK1B in a 1:3 proportion. Nontransfected GT-GFP cells were also analyzed as an additional control (Fig. 5, A and B). The flow of GT was determined by fluorescence recovery at 200 s after bleaching a selected area (Fig. 5 C). Notably, fluorescence was recovered at almost similar levels in controls and in AK1-expressing cells (~50%), whereas it was incomplete in cells expressing the small AK1B fragment (~25%). Determination of the GT mobile fraction revealed that in the presence of the AK1B fragment, the enzyme mobility between stacks was reduced by 40% (Fig. 5 C). These results indicate that the Golgi ribbon of AK1B-expressing cells is interrupted, possibly because of stacks being disconnected. On the other hand, the expression of the large AK1 fragment did not significantly impair GT mobility between stacks, suggesting the possibility of generating an intact Golgi ribbon far from the CTR.

Golgi ribbon reassembly in cells expressing AK1- and AK1B-truncated mutants

To gain insights into the GA formation process, we used time-lapse microscopy to compare GA reassembly after NZ treatment in control, AK1-, or AK1B-expressing cells (Fig. 6).

RPE-1 cells grown on gridded dishes were either transfected with GT-mCherry (control) or cotransfected with GT-mCherry and GFP-AK1 or GFP-AK1B constructs. After NZ removal, double-transfected cells were recorded for several hours (Fig. 6, left) and then fixed and processed by IF to determine CTR position (Fig. 6, right).

In agreement with experiments by others (Miller et al., 2009), GA elements in control cells underwent peripheral fusion (G stage) before being translocated toward the cell center (C stage; Fig. 6 A). A decrease in number and an increase in size of GA ministacks during the first hour of drug washout were noteworthy. 3 h after NZ washout, all GA clusters appeared located around the CTR (Video 1). In parallel experiments on fixed cells, an intact Golgi ribbon could be observed at this time (Fig. 6 A, right). The GA reassembly in cells expressing the large N-terminal fragment AK1 proceeded significantly slower than in control cells (Fig. 6 B). Under such conditions, GA elements apparently fused at the cell periphery, although at a lower rate than in control cells. In addition, GA elements failed to concentrate at the cell center, and 5 h after washout, some elements still remained separated from the rest (Video 2). Collectively, our results suggested that, although less efficiently than in the control cell, the G stage occurred in these cells, whereas the C stage did not occur, leading to the Golgi ribbon forming at random locations with respect to the CTR. Finally, in cells expressing the AK1B fragment (Fig. 6 C), a concentration of GA ministacks around the CTR was detected earlier than in control cells (Fig. 6, A and C, compare reassembly in images after 32 min), but GA elements at the cell periphery did not increase in size at any time, suggesting that peripheral fusion was inhibited. Ministack clustering occurred mostly in a radial manner, which is consistent with a role of the radial centrosomal MT array in this movement (Video 3). Thus, only the C stage seems to take place in these cells (Fig. 6, right images show the same experiment in fixed cells).

Together with FRAP experiments, our data indicate that selective perturbation of one of the two stages of the Golgi ribbon formation process produces strikingly different effects on Golgi organization. Inhibition of ministack fusion at the cell periphery (G stage) by the AK1B fragment results in a properly localized, but fragmented, Golgi ribbon, whereas inhibition of central concentration (C stage) by AK1 fragment without preventing ministack fusion produces a mislocalized Golgi ribbon (see Discussion for a model).

Defective secretion in AK1- and AK1B-transfected cells

To address the significance of GA integrity or positioning in secretion, we first monitored ER to plasma membrane (PM) transport of the temperature-sensitive mutant of VSVG-GFP in control, AK1-, or AK1B-transfected cells (Fig. 7, A and B). VSVG-GFP was detected at the PM by incubating with an ectodomain antibody during the last 30 min of a 60- or 100-min period after the shift at a permissive temperature (Fig. 7 A). VSVG-GFP accumulated at the cell surface under all conditions. Quantification revealed no significant differences between control and transfected cells (Fig. 7 A, bottom). In parallel, transfected cells were fixed at different time points after the temperature shift (Fig. 7 B). Trafficking from the ER to the GA was apparently unaffected in mutant-expressing cells even when the GA was localized away from the CTR. It should be noted that endoplasmic reticulum exit sites (ERES) concentrated around the GA regardless of their positioning inside the cell (Fig. S5). VSVG-GFP was transported from the ER to the PM in both AK1- and AK1B-expressing cells, although a slight delay was apparent in VSVG transport from the GA to the PM (Fig. 7 B, right column). In agreement with previously published data (Miller et al., 2009; Yadav et al., 2009), our results indicate that neither Golgi ribbon integrity nor positioning are critical for global secretion.

To study directed secretion, we analyzed by live imaging the post-GA trafficking of secreted fluorescently labeled neuropeptide Y (NPY) in control or transfected cells induced to migrate by wounding (Fig. 7 C). Cells were recorded for 2 min (Fig. 7 C, left column; and Videos 4, 5, and 6), and then, all images were overlaid to visualize pathways defined by post-GA vesicles (Fig. 7 C, central column). Finally, selected individual NPY-containing vesicles were tracked from the first to the last frame (Fig. 7 C, right column). In control cells, many NPY-containing vesicles leaving the GA and targeting the PM at the leading edge were observed. In contrast, expression of each AKAP450-truncated mutant reduced the number of NPY vesicles formed at the TGN in the same period of time, and delivery to the leading edge was also impaired (Fig. 7 C and Videos 5 and 6). Tracking of individual vesicles revealed that vesicle formation and movement rates were diminished in cells expressing AKAP450 fragments. Because both mutants induced a similar trafficking phenotype, the deficiency of GA to PM transport is most probably reflecting a role of Golgi-nucleated MTs in facilitating post-Golgi trafficking (Miller et al., 2009).

Pericentrosomal GA positioning is critical for cell polarization and directed migration

To study the specific role of Golgi positioning and integrity in cell polarity, scratch wounding was performed on control, AK1-, and AK1B-transfected cells (Fig. 8 A). The CTR and GA were counted as oriented when most of the labeling was located within the 90° angle facing the wound (Fig. 8 A). As expected, ~80% of control cells had already oriented both the CTR and GA at 3 h after wounding (Fig. 8 B). In AK1-expressing cells, however, the percentage of reoriented GA was only 45%, even 8 h after wounding. Interestingly, the same number of cells had reoriented the CTR at this time point. Finally, although the kinetics of GA and CTR reorientation in AK1B-expressing cells was slower, 8 h after wounding, the number of reoriented cells was only slightly reduced with respect to control cells (<10%).

To test for potential migration defects, an identical experiment was performed, but control, GFP-AK1–, or GFP-AK1B–expressing cells were recorded by phase-contrast live microscopy for 17 h after wounding (Fig. 8 C and Videos 7, 8, and 9). 13 control (Fig. 8 C, top), AK1 (Fig. 8 C, middle)- or AK1B (Fig. 8 C, bottom)-transfected cells were false colored and tracked from the first to the last frames of the video. As expected, control cells exhibited persistent directional migration until the closure of the gap. Strikingly, AK1-transfected cells

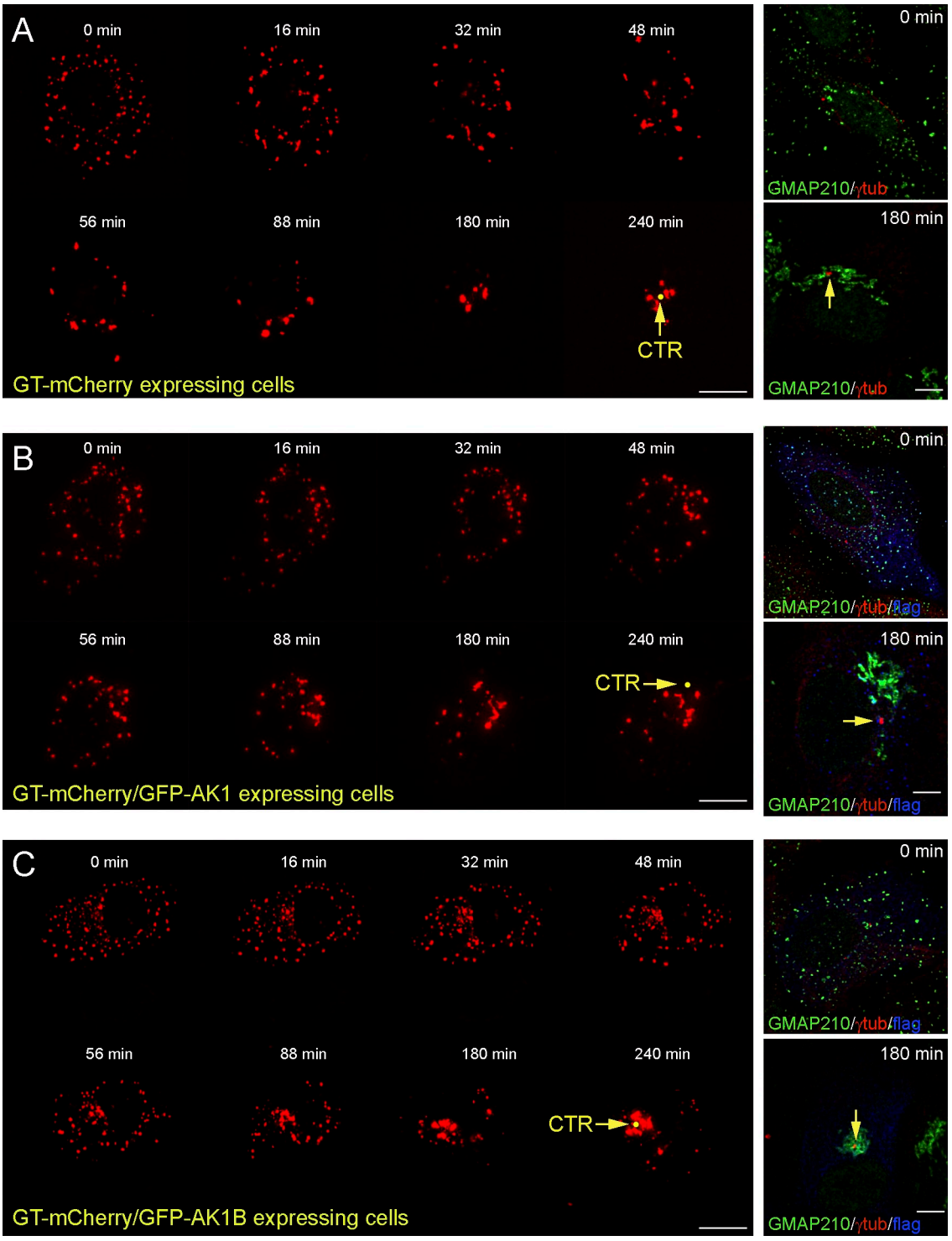

Figure 6. **Reassembly of the GA after NZ washout is perturbed at different stages in AK1- and AK1B-transfected cells.** (A–C) RPE-1 cells expressing GT-mCherry (A) or coexpressing GT-mCherry and either GFP-AK1 (B) or GFP-AK1B (C) were treated with NZ for 3 h and incubated at 4°C for 1 h in the presence of the drug. After washout, cells were recorded by video microscopy. Time after NZ removal is shown. (A) Video frames illustrating two-step reassembly of the GA in control cells. Golgi elements partially fuse in the cell periphery before being translocated toward the CTR. (B) In AK1-transfected cells, Golgi elements fuse in the cell periphery at lower rates than in control cells and do not apparently move toward the cell center. (C) In AK1B-transfected cells, Golgi elements are radially translocated toward the CTR without peripheral fusion. (right) An identical experiment in fixed cells. CTR position is indicated (yellow arrows). γtub, γ-tubulin. Bars, 3 µm.

were unable to migrate in a directional manner: cells moved less and in a wrong direction, probably as a consequence of the lack of GA–CTR polarization toward the leading edge. Finally, cells expressing the AK1B mutant exhibited reduced mobility without any obvious effect on the directionality of migration. Quantification of the cell-covered area during wound healing

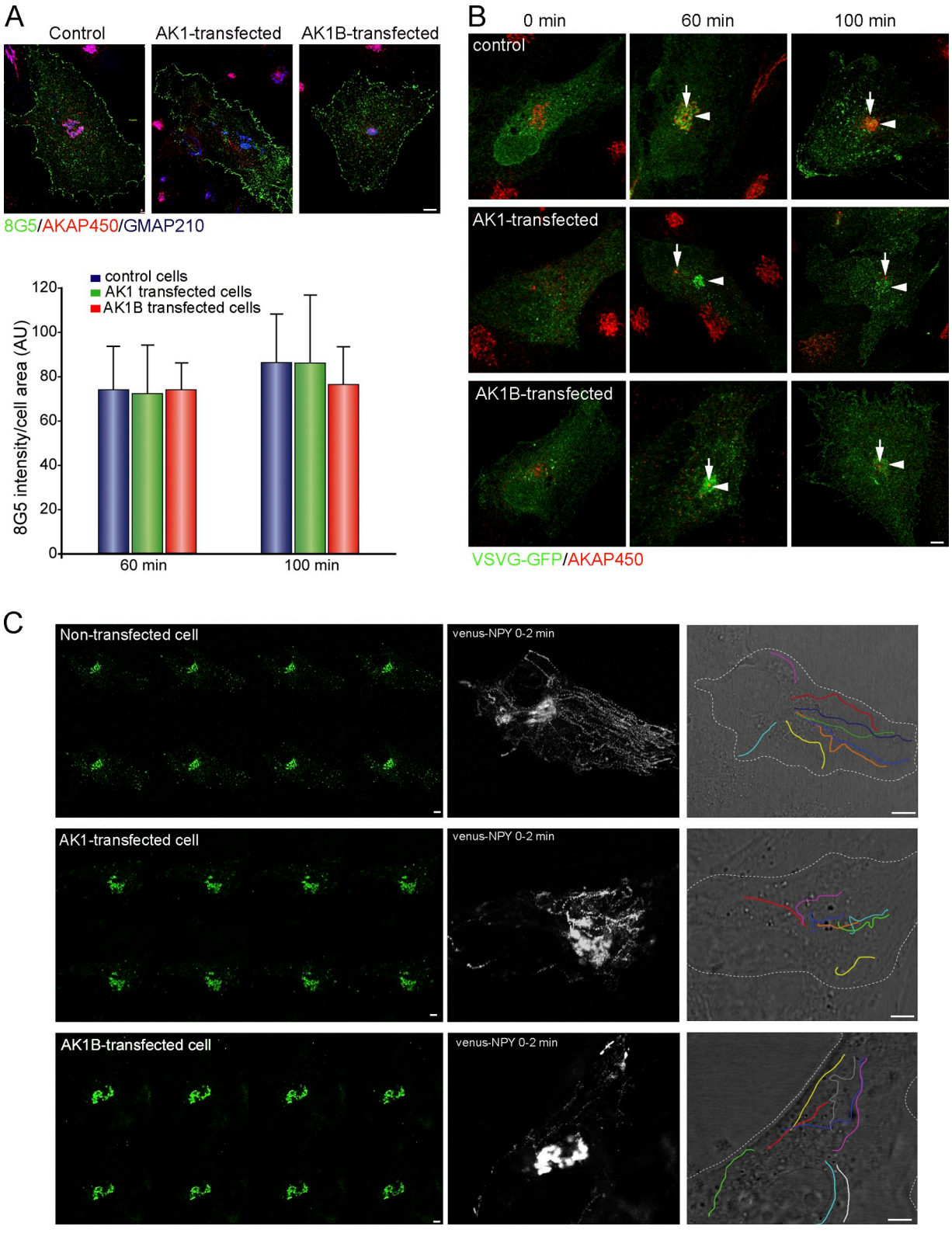

Figure 7. **Membrane trafficking in AK1- and AK1B-transfected cells.** (A) RPE-1 cells were transfected with VSVG-GFP (control) or cotransfected with VSVG-GFP and either flag-AK1 or flag-AK1B as indicated. VSVG-GFP was detected at the PM by incubating with the ectodomain antibody 8G5 during the last 30 min of a 60- or 100-min period after the shift at a permissive temperature. Cells were then fixed and stained as indicated (top images). 8G5 labeling was also quantified by using MetaMorph (n = 20 for each condition). Error bars indicate standard deviations. (B) Identical experiment as in A, but at different times after the permissive temperature shift, cells were fixed and stained as indicated. Arrows indicate the CTR, and arrowheads show the GA. (C, left) Video frames showing translocation of venus-NPY–containing vesicles in control cells, AK1-, or AK1B-expressing cells. (middle) Venus-NPY images recorded over 2 min were overlaid to visualize vesicle tracks. (right) Randomly selected particles were tracked for 2 min, and movement tracks are represented in different colors over a phase-contrast image of the recorded cell. Dashed lines indicate the cell border. Bars: (A and B) 10 µm; (C) 2.5 µm.

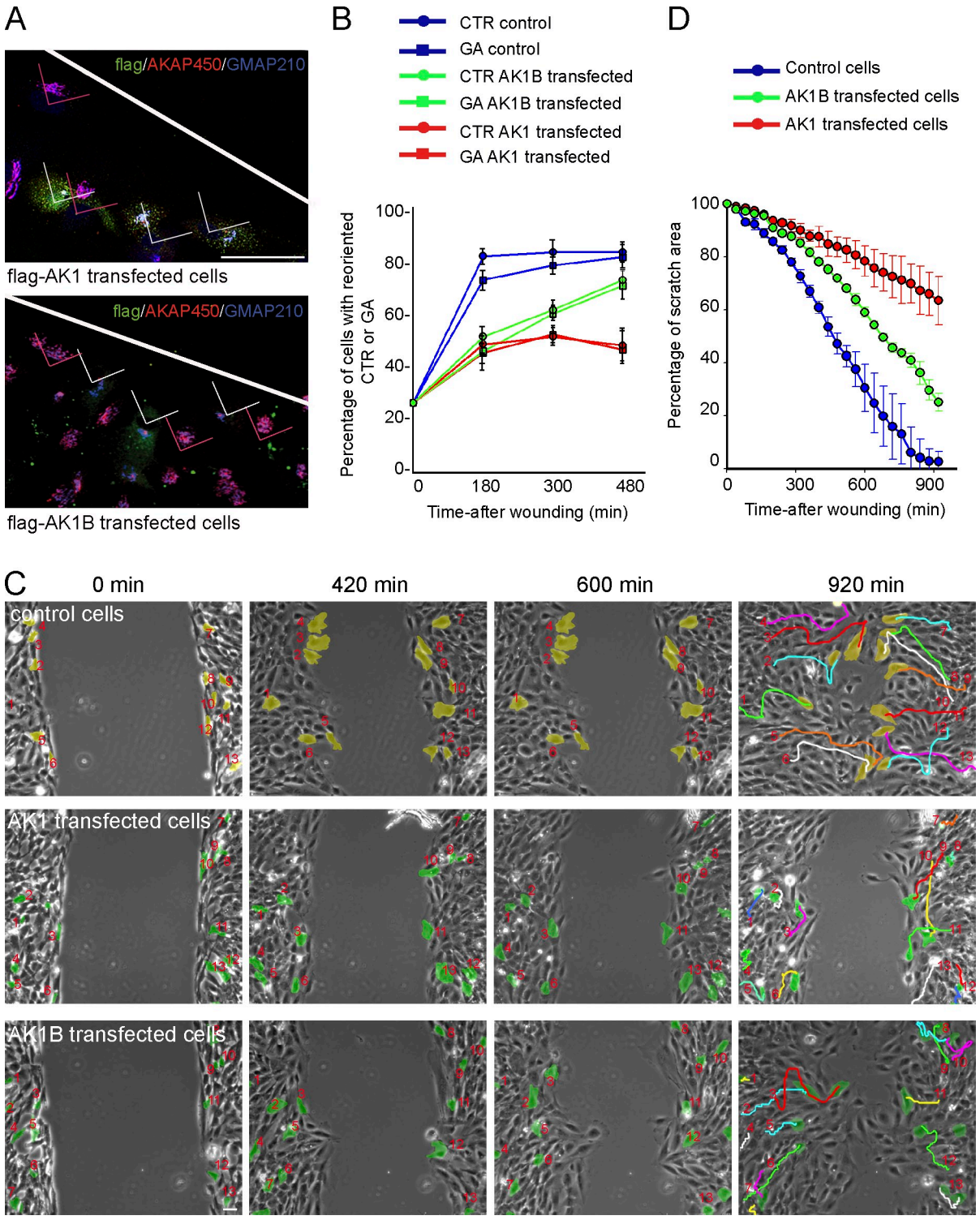

Figure 8. **Cell polarization and migration analysis in AK1- and AK1B-expressing cells.** (A) Reorientation of the CTR and the GA after wounding in AK1 (top)- and AK1B (bottom)-transfected cells. The white lines indicate the scratch orientation. Pink or white angles indicate nontransfected or transfected cells, respectively. (B) Graph showing the percentage of control, AK1-, and AK1B- transfected cells with the CTR (circles) or the GA (squares) reoriented toward the wound at each time point. Random orientation is expected to be 25%. $n \geq 80$ cells for each condition from two independent experiments. (C) Wound-healing assays in either control (top row), AK1 (middle row)-, and AK1B (bottom row)-transfected cells. Frames from time-lapse phase-contrast videos at the indicated times are shown. 13 selected cells were false colored and numbered to better visualize their movement. Tracks indicating frame by frame movement of cells are overlaid in right images. (D) Quantitative analysis of wound-healing assays by using the WimScratch software (Wimasis). Graph represents the percentage of scratch area at each time point in control, AK1-, and AK1B-expressing cells. Values are from three independent experiments. Error bars indicate standard deviations. Bars, 12.5 µm.

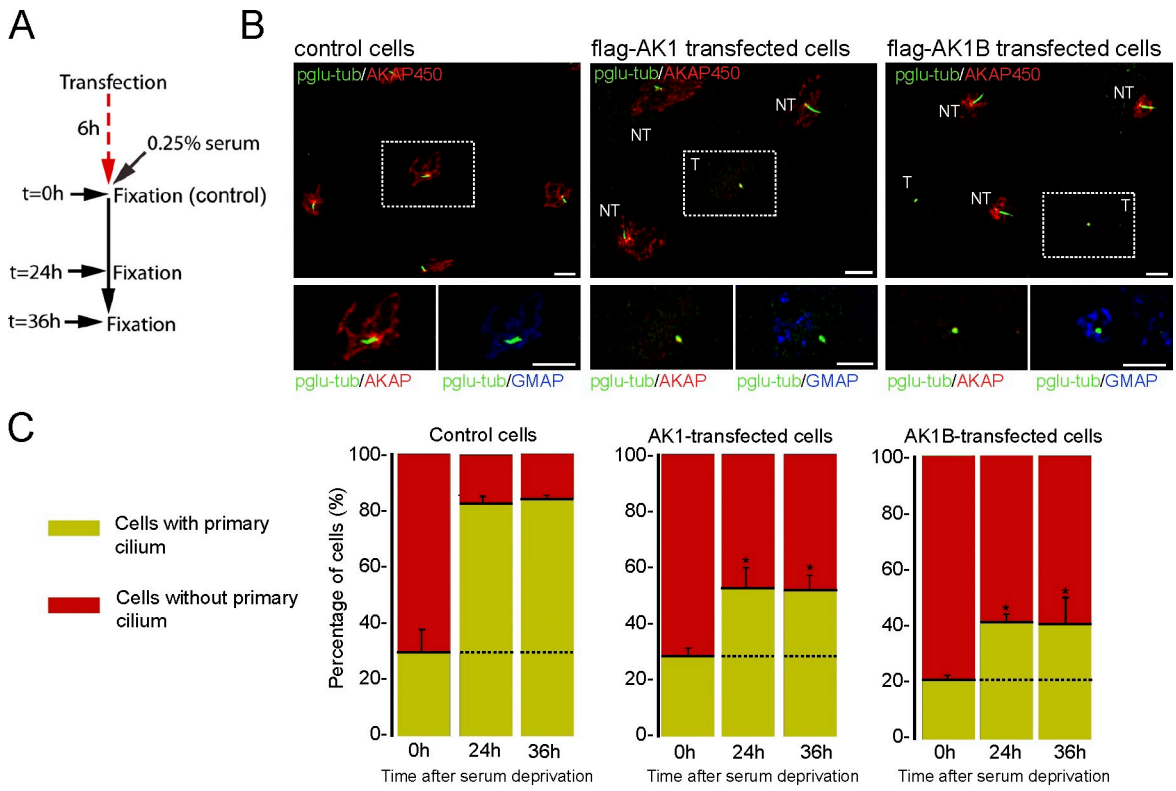

Figure 9. **Primary cilium formation is severely impaired in AK1 or AK1B fragment–expressing cells.** (A) Schematic of the procedure used for primary cilium induction. (B) Representative images of control (right), flag-AK1 (middle)–, and flag-AK1B (left)–transfected cells maintained in 0.25% serum for 36 h and triple labeled for polyglutamylated tubulin (pglu-tub), AKAP450, and GMAP210. Double merged images are as indicated. Boxes are enlarged on the bottom. T, transfected cell; NT, nontransfected cells. Bars, 7.5 µm. (C) Bar graphs showing the increase on the percentage of cells with primary cilium at 0, 24, and 36 h after serum deprivation. Dotted lines indicate the percentage of cells containing a cilium before starvation. n = 300 from three independent experiments (*, $P < 0.001$; Tukey HSD). Error bars indicate standard deviations.

is shown in Fig. 8 D. These results demonstrate that pericentrosomal positioning of the GA is essential for mammalian cells to properly respond to directional migration signals.

Both integrity and position of the GA are required for primary cilium formation

Primary cilium assembly involves MT organization and polarized membrane trafficking (Satir et al., 2010). We were eager to investigate whether perturbations in GA position or integrity block primary ciliogenesis induced by serum deprivation. 6 h after transfection with AK1 or AK1B constructs, cells were serum deprived for different periods of time as represented in Fig. 9 A. Cells were fixed and stained as indicated (Fig. 9 B), and the number of ciliated cells was determined for each condition by immunostaining with antipolyglutamylated (Fig. 9 B) or acetylated tubulin (not depicted) antibodies. Quantification revealed that ∼30% of cells already contained a primary cilium at the moment of starvation. In control cells, the number of ciliated cells increased from 30 to 80% after 24 h in the absence of serum. In contrast, in AK1- or AK1B-transfected cells, only 20% of transfected cells were able to develop a cilium, even after 36 h of serum deprivation. This dramatic reduction in the ability to generate a primary cilium in AK1- and AK1B-transfected cells indicates that both the Golgi integrity and pericentrosomal position are essential to form cilia in epithelial cells.

Discussion

The correct morphology and positioning of the GA in mammalian cells is achieved by the cooperation of several factors, including MTs growing from both the GA and the CTR, dynein activity, and peripheral GA proteins, such as GM130 and its partner GRASP65 among others (Puthenveedu et al., 2006; Miller et al., 2009; Sengupta et al., 2009). The combined capacity of AKAP450 for binding GM130, γ-tubulin small complex, and dynein–dynactin makes it a compelling candidate for being a master factor in this process. By specifically interfering with these interactions using the dominant effect of partial constructs, we have set the experimental conditions to generate a pericentrosomal fragmented GA or, alternatively, a mislocalized intact Golgi. A summary of phenotypes induced by the N-terminal AKAP450 fragments is shown in Table I.

We have identified the GA-targeting GM130-binding domain of AKAP450 at its N terminus. Only truncated mutants containing this motif, i.e., AK1 and AK1B, could bind to the GA and displace endogenous AKAP450, indicating that it is probably the only GA-binding domain of the protein. The ability of AK1B- and AK1-truncated proteins to dissociate AKAP450 from GA membranes allowed us to evaluate the relevance of AKAP450 Golgi association without affecting other AKAP450-dependent processes (El Din El Homasany et al., 2005; Robles-Valero et al., 2010; Sehrawat et al., 2011). Effects induced by AK1B expression

Table I. **Phenotypes induced by the expression of N-terminal AKAP450 fragments**

AKAP450 fragments	Golgi integrity	Golgi positioning	Secretion	CTR/GA reorientation	Directional migration	Primary cilium formation
AKAP450 1–3,899 aa	+++	+++	+++	+++	+++	+++
AK1 domain 1–1,029 aa	++	−	++	+/−	−	−
AK1B domain 159–463 aa	−	+++	++	++	+	−

+++, normal phenotype; ++, slightly affected; +, mildly affected; +/−, moderately affected; −, strongly affected.

on GA morphology were reminiscent of those induced by depletion of CLASP proteins, suggesting that they were mainly caused by inhibition of the GA-dependent nucleation of MTs. The large N-terminal mutant corresponding to the first quarter of the protein and the smaller AK1B share the capacity to bind GA, to displace AKAP450, and to inhibit MT nucleation at the GA. Yet, the phenotypes on the GA were strikingly different. The additional capacities of AK1 with respect to AK1B to bind MTs and to interact with p150*glued* seem to be responsible for this difference.

FRAP analysis revealed a significantly restricted lateral diffusion in the condensed GA observed in AK1B-expressing cells compatible with a fragmentation of the GA into disconnected stacks. On the contrary, fluorescence recovery in AK1-transfected cells appeared similar to control cells. In both cases, the GA did not show defects on cis–trans polarity, mislocalization of Golgi proteins, or inhibition of drug-induced Golgi disassembly/reassembly, indicating that the cisternal structure was not affected. Moreover, ERES accumulated close to the GA in both AK1- and AK1B-expressing cells, suggesting active ER to GA transport. Finally, VSVG-GFP secretion was not significantly perturbed. Altogether, these data indicate that AK1- and AK1B-transfected cells retain normal Golgi structure and secretion kinetics, thus establishing conditions to test the role of ribbon integrity and positioning in polarization, migration, and primary cilium formation.

Data from our in vivo NZ recovery experiments are in agreement with a two-stage model for ribbon assembly (Miller et al., 2009). The pattern of GA reformation in AK1B-expressing cells was similar to that of CLASP-depleted cells, further indicating that these defects are caused by the inhibition of GA-associated MT nucleation. Under these conditions, the G stage at the cell periphery did not take place. GA ministacks could, however, be translocated toward the cell center, leading to the concentration of disconnected GA ministacks around the CTR. In addition to AKAP450 (Kim et al., 2007), several proteins have been shown to recruit dynein to the GA, including Bicaudal D, ZW10, LIS1, NDE1, and NDEL1 (Kardon and Vale, 2009), and might support central translocation of GA elements in the absence of GA-associated AKAP450. Interestingly, transfection of LIS1, NDE1, and NDEL1 caused the GA to become more compact around the CTR, just like AK1B expression does. This phenotype was proposed to be caused by increased dynein activity (Lam et al., 2010). The GA-associated AKAP450 network might be restricting dynein activity under normal circumstances, thus leading to a more extended GA ribbon.

On the contrary, AK1-containing elements were unable to be translocated toward the cell center and eventually fused into a ribbon in the cell periphery. How this can be possible is a challenging question. For a ribbon to be formed, GA elements need to be brought into close proximity, thereby allowing the fusion machinery to proceed. MT-driven colocalization of membranes is crucial for this machinery to work: in the absence of MTs, GA stacks are no longer held together, whereas fusion proteins remain associated to membranes. Because AK1 binds to MTs in addition to GA membranes, one can safely assume that binding of AK1 to GA results in an increased MT-binding activity of GA elements, probably through the recruitment of p150*glued* by AK1. We thus favor a model in which the ability of GA membranes to bind MTs through AK1 considerably increases the chances of GA ministacks to progressively find themselves close to each other: instead of being distributed randomly in a 3D space, which would give virtually no chance to GA ministacks to encounter each other, GA ministacks would all be distributed along linear MTs. In agreement with this view, the process was rather slow (Fig. 6), suggesting that it is not an active motor-driven mechanism but rather a passive diffusion along MTs. This is further supported by the fact that the progressive fusion in a GA ribbon at the cell periphery does not involve unidirectional movement of GA elements apparently (Video 2) and, more compellingly perhaps, by the absence of translocation of GA elements to the cell center. This feature could be explained by considering that increased AK1-associated p150*glued* interferes with dynein activity. Indeed, in vitro data have suggested that the p150*glued* MT-binding cytoskeleton-associated protein–Gly domain might act as a brake that inhibits dynein motility (Steinmetz and Akhmanova, 2008). These results also suggest that pericentrosomal concentration of GA stacks powered by dynein is not a prerequisite to form a ribbon. The MT minus end–directed transport of GA elements ensures that the ribbon forms around the CTR but is not required for fusion if an alternative mechanism is provided to bring GA fragments together. As a matter of fact, in taxol-treated cells in which MT polarity is often reversed and MT minus ends concentrated close to the PM, a Golgi ribbon can be formed at the cell periphery (Fig. S2).

Our results also imply that GA-associated MT nucleation might not be critically required for fusion if CTR-nucleated cytoplasmic MTs can be used for favoring tangential linking of GA stacks as previously proposed (Rios et al., 2004). Such a mechanism might explain how the pericentrosomal Golgi

ribbon organization is achieved in some cell lines, such as HeLa cells, in which the GA does not apparently nucleate MTs. It should be noted that not only MT nucleation capacity but also fusion machinery might differ between cell lines. Thus, GRASP65 depletion did not result in Golgi fragmentation in RPE-1 cells (unpublished data; Rivero et al., 2009) contrary to what has been reported in HeLa cells (Puthenveedu et al., 2006).

An important outcome of proper Golgi ribbon organization is to support polarized membrane traffic in motile cells. Reorientation of the GA/CTR in the direction of cell migration places the GA in the correct position to send cargo to the leading edge. The current model is that directional trafficking from the polarized Golgi ribbon supported by GA-derived MTs is required for directional cell motility. Thus, blockade of anterograde membrane traffic (Prigozhina and Waterman-Storer, 2004), dispersion of the Golgi ribbon (Yadav et al., 2009), or inhibition of GA-associated MT nucleation (Miller et al., 2009) perturbs directional cell migration. These studies uncovered a role for GA morphology and positioning facing the leading edge in cell migration, but they did not address the relevance of GA/CTR association. Our data indicate that pericentrosomal position of the GA is a more determinant factor for cell polarity and directional migration than GA morphology or GA-associated MT nucleation. Because in both AK1B- and AK1-expressing cells, GA-derived MTs were lacking and secretion was perturbed to the same extent, the more severe phenotype on cell polarization and migration displayed by AK1-expressing cells is probably caused by mislocalization of the Golgi ribbon. Interestingly, not only the GA but also the CTR failed to reorientate in these cells, suggesting that the pericentrosomal GA contributes to CTR reorientation. Accordingly, CTR polarization could not be achieved when GA polarization was inhibited by expression of some GRASP65 mutant forms (Bisel et al., 2008). Dislocation of the polarity axis induced by the AK1 fragment resulted in an aberrant migration pattern with cells moving in the wrong direction. How the GA and the CTR are coordinately repositioned toward the leading edge is still unclear. However, our data reveal an active role of the GA in this process, possibly through the AKAP450 network itself.

The formation of the primary cilium induced by serum deprivation was shown to be the most critically dependent process on proper location and/or integrity of the GA. It is known that the building and maintenance of a cilium depend on the trafficking of membrane vesicles, whereas the mechanisms by which membrane proteins and lipids are specifically targeted to the cilium are largely unknown (Pitaval et al., 2010; Satir et al., 2010). It has been proposed that ciliary cargo might be recruited into vesicles indirectly through interactions with other ciliary proteins that serve as adaptors. The best candidate for such an adaptor is the intraflagellar transport protein IFT20 whose depletion prevents ciliogenesis. IFT20 not only localizes at the cilium but also at the cis-GA where it is recruited by GMAP210 (Follit et al., 2008). The pools of GA-associated or basal body–associated IFT20 are in dynamic exchange. Thus, the close proximity of the GA to the CTR during ciliogenesis surely facilitates the delivery of vesicles to the base of the cilium. The dramatic reduction in the number of ciliated cells in AK1-expressing cells supports this possibility. On the other hand, GMAP210 is not only important for ciliogenesis but for maintaining GA integrity as well, probably by participating in the formation of connecting cis-cisternae (Cardenas et al., 2009). How GMAP210 accomplishes these two functions is an intriguing question. One interesting possibility is that the two functions are mutually dependent. If this were true, disrupting the Golgi ribbon would perturb cilium formation as it occurs in AK1B-expressing cells. This would explain primary cilium resorption during mitosis: because the GA fragments during G2, the dual function of GMAP210 would ensure that trafficking from the GA to the cilium is blocked during mitosis entry.

As a whole, our work demonstrates a role of the AKAP450–GM130 complex in organizing the Golgi ribbon around the CTR. How this interaction is regulated during the cell cycle and how GA-associated MT nucleation is inhibited at the onset of mitosis to ensure the proper formation of the spindle are interesting questions that deserve attention for the future.

Materials and methods

Cell culture, treatments, and antibodies

Immortalized human pigment epithelial cells hTERT–RPE-1 (Takara Bio Inc.) and immortalized nonmalignant human breast epithelial MCF10A cells were grown under standard conditions. To generate an hTERT–RPE-1 cell line with a fluorescence-labeled GA, we used the pAcGFP1-Golgi vector, which encodes a fusion protein consisting of the N-terminal 81 aa of the human β 1,4-GT directly upstream of the GFP from *Aequorea coerulescens* (GT_{TM}-GFP). This sequence was subcloned into the bicistronic pIRESneo vector, and the new construct was transfected in hTERT–RPE-1 cells by using Lipofectamine and then selected with G418 for 4–6 wk. Finally, cell population was sorted in a cell-sorting system (FACSAria; BD), and only cells expressing high levels of the protein were maintained (Cardenas et al., 2009). Treatments were with 10 µM NZ (Sigma-Aldrich) for 2 h, 10 µM taxol (paclitaxel; Sigma-Aldrich) for 5 h, or 5 µg/ml brefeldin A (LC Laboratories) for 90 min. Antibodies used in this paper were rabbit anti-AKAP450 (Rivero et al., 2009), human sera against GMAP210 and Golgin-245 (Rios et al., 2004), and GT335 (Wolff et al., 1992). Monoclonal anti–α-tubulin, anti–γ-tubulin (clone GTU-88), and anti-flag M2 were obtained from Sigma-Aldrich, anti-GFP was obtained from Abnova, and anti-GM130, anti-AKAP450, and anti-Sec31 were obtained from BD. Rat monoclonal anti–α-tubulin was purchased from Abcam, and rabbit polyclonal anti-GFP was purchased from Immunology Consultants Laboratory, Inc. Rabbit anti-GM130 and mouse BW8G5 were gifts from Y. Misumi (Fukuoka University, Jonan-ku, Fukuoka, Japan) and W.E. Balch (The Skaggs Institute for Chemical Biology, La Jolla, CA), respectively. All secondary antibodies conjugated to DyLight fluorophores were obtained from Jackson ImmunoResearch Laboratories, Inc.

Constructions, transfections, and RNA interference

To generate GFP- or flag-tagged versions of truncated mutants, corresponding sequences were amplified by PCR and cloned in both pEGFP-C and pCS2-flag plasmid series, respectively. GT-mCherry, Venus-NPY, and YFP-GM130 were provided by I. Kaverina (Vanderbilt University Medical Center, Nashville, TN), B. Goud (Unité Mixte de Recherche 144, Institut Curie, Paris, France), and V. Malhotra (Centre de Regulació Genòmica, Barcelona, Spain), respectively. Cells were transfected with Lipofectamine 2000 (Invitrogen) according to manufacturer's instructions. Unless otherwise stated, cells were processed 16 or 24 h after transfection for GFP-tagged and flag-tagged proteins, respectively. To deplete AKAP450 and GM130 expression, we used a mixture of two siRNAs (5′-AACTTTGAAGTTAACTATCAA-3′ and 5′-ATATGAACACAGCTTATGA-3′ for AKAP450 and 5′-CAATGCTGCTACTCTACAATT-3′ and 5′-CAATGCTGCTACTCTACAATT-3′ for GM130). Duplexes were obtained from Sigma-Aldrich or Thermo Fisher Scientific.

Western blotting (WB), IP, MT taxol purification, and MT regrowth assays

For WB, proteins were separated by SDS-PAGE, and gels were transferred to nitrocellulose filters and blocked for 1 h at 37°C in TBST (10 mM Tris/HCl, pH 7.4, 150 mM NaCl, and 0.1% [vol/vol] Tween 20) containing 5% (wt/vol) nonfat dried milk. Filters were then incubated for 1–2 h at 37°C

with the primary antibody in the same buffer, washed, and incubated for 45 min at 37°C with the secondary anti–rabbit or anti–mouse IgG antibodies conjugated with peroxidase (GE Healthcare). For co-IPs, transfected cells were harvested 16 or 24 h after transfection and lysed in NP-40 buffer (10 mM Tris/HCl, pH 7.4, 150 mM NaCl, 10% [vol/vol] glycerol, 1% [vol/vol] NP-40, 1 mM PMSF, and 1 µg/ml each of pepstatin, leupeptin, and aprotinin) for 20 min at 4°C and then for 3 min at 37°C. The extract was centrifuged at 20,000 *g* for 20 min, and the soluble fraction was preadsorbed with an irrelevant antibody on protein A–Sepharose or protein G–agarose for 2 h. Then extract was incubated with beads alone or immunoprecipitated with 0.5–1 µl of the antibody of interest on protein A–Sepharose or protein G–agarose for another 2 h. After washing beads, pellets were analyzed by WB.

For MT-pelleting assays, extracts were prepared by adding BRB80 buffer (80 mM Pipes, pH 6.8, 1 mM $MgCl_2$, and 1 mM EGTA) to cell pellets. Samples were centrifuged at 20,000 *g* at 4°C for 20 min to pellet unbroken nuclei, and the supernatant was transferred to a clean tube. The extract was precleared by ultracentrifugation at 189,000 *g* for 20 min at 4°C, and the supernatant was transferred immediately to a clean tube on ice. 0.5 mM MgGTP and 2 mM MgATP were added, and extracts were warmed to RT. Then, extracts were incubated for 2–3 min with 5 µM taxol before an additional 15 µM taxol was added. In addition, 0.2 mg/ml taxol-stabilized MTs from commercial tubulin (Cytoskeleton) was added and incubated for 30 min at 30°C. The polymerized mixture was layered onto a 1-M sucrose cushion in BRB80 buffer containing 0.5 mM ATP, protease inhibitor cocktail, and 10 µM taxol. MTs were pelleted at 69,500 *g* for 20 min at 22°C. The supernatants were removed and saved for WB. The MT pellet was washed twice in BRB80 and resuspended in SDS loading buffer to 0.2 vol of the supernatant. All samples were analyzed by WB. For MT regrowth assays, cells were incubated with NZ for 3 h at 37°C and then for an additional 1 h on ice. Alternatively, MTs were depolymerized on ice for 60 min. Cells were rinsed with ice-cold medium, and warmed medium was added to induce MT regrowth. All MT regrowth experiments were performed at RT.

IF and image analysis

Cells were grown on glass coverslips and fixed with cold methanol for 6 min at –20°C. For GFP and mCherry fluorescence, cells were fixed in 3% PFA for 10 min and permeabilized with PBS–0.1% Tween–0.5% Triton X-100 for 5 min at RT. For CYTOOchip experiments, control, AK1-, and AK1B-transfected RPE-1 cells were seeded on small Y-shaped micropatterns (CYTOO SA) following the manufacturer's protocol. In brief, cells were collected by trypsinization and diluted to a concentration of 15,000 cells/ml. Then, 60,000 cells were dispensed into each micropattern and allowed to sediment for 10 min under the hood before moving them to the incubator. After 45 min, the medium was changed, the coverslip surface was gently flushed, and finally, cells were allowed to spread for 5 h before fixation. Cells were examined under a motorized upright wide-field microscope (DM6000B; Leica). Confocal images were captured by a confocal microscope (TCS SP5; Leica) using an HCX Plan Apochromat λ blue 63×/1.4 NA oil objective at 22°C, and they correspond to maximal projections except in Fig. 7 (A and B) in which optical sections are shown. Image analysis was performed using the Leica and Photoshop (Adobe) software. Intensity level, contrast, and brightness of images were adjusted using these programs. Relative GA recruitment of mutants was calculated by dividing the mean pixel density measured in three areas of interest placed over the GA by that measured in a region of the cytoplasm outside the GA. For calculation of the fluorescence intensity profiles, images were processed with MetaMorph Offline 7.1.7.0 (Molecular Devices) using the command Linescan to view the intensity values along a given line in graphical format. The GA diameter and CTR–GA distance measurements were analyzed using Photoshop and MetaMorph softwares. A straight line connecting the center of circumferences circumscribing the GA and the CTR was measured to calculate the CTR–GA distance. GA diameter was used as an index of GA circularity.

FRAP

A stable GT-GFP RPE-1 cell line was used. Cells were plated onto 35-mm glass-bottom dishes (MatTek) and transfected with mCherry-centrin or cotransfected with mCherry-centrin and either AK1- or AK1B-flag mutants in a 1:3 proportion (one molecule of the mCherry-centrin vector for three molecules of the corresponding mutant-expressing vector). Only cells expressing mCherry-centrin as the limiting factor were analyzed. FRAP was performed using a laser-scanning confocal microscope (TCS SP5) equipped with an environmental control system set to 37°C and 5% CO_2. Cells were cultured in phenol red–free DME/F12 (Sigma-Aldrich) and visualized using the argon laser line (488 nm) with an HCX Plan Apochromat λ blue 63×/1.4 NA oil objective. Prebleached images were taken for 3 s (1 s/frame), and the selected GA area was bleached for 1 s using a pulse of the 488-nm laser line at maximal intensity. After bleaching, fluorescence images were then recorded every 1 s for 200 s (1 s/frame). Normalization was set between the values before bleaching and the first time point after bleaching. After background correction, the GT-GFP mobile fraction of each cell was determined as the ratio between the mean intensity reached in the plateau of the fluorescence recovery and the mean intensity of a selected GA area in a neighbor cell.

VSVG trafficking

RPE-1 cells were grown on coverslips and either transfected with VSVG-GFP or cotransfected with either VSVG-GFP and flag-AK1 or with VSVG-GFP and flag-AK1B. 16 h after transfection, cells were incubated at 40°C for 4 h. Then, 100 µg/ml cycloheximide (Sigma-Aldrich) was added to the medium, and cells were maintained for an additional 2 h at 40°C. Cells were then transferred to 32°C and fixed at different time points. For 8G5 staining, living cells were incubated with the ectodomain antibody for the last 30 min of a 60- or 100-min period after transferring cells to 32°C. The ratio of total fluorescence to cell area was used to calculate the extent of VSVG transport. Both intensity and cell area were measured using MetaMorph software.

In vivo Venus-NPY trafficking and Golgi reassembly experiments

For imaging experiments, cells were cultured in phenol red–free DME/F12. To follow post-GA trafficking, we transfected RPE-1 cells with fluorescently labeled Venus-NPY or cotransfected Venus-NPY with either flag-AK1 or flag-AK1B fragments. Cells were plated onto Culture Insert (IBIDI) over glass-bottom dishes and serum starved for 16 h. 3 h after serum addition, cells were recorded with a laser-scanning confocal microscope (TCS SP5) equipped with an environmental control system set to 37°C and 5% CO_2 and using an HCX Plan Apochromat λ blue 63×/1.4 NA oil objective at 22°C. 2-min NPY vesicle tracks were recorded for each transfected or cotransfected cell localized in the first row facing the leading edge. The vesicle tracking was analyzed for eight cells in each experiment. For GA reassembly experiments, RPE-1 cells were plated onto µ-Dish^{35mm,high} with Grid-500 (IBIDI) and transfected with GT-mCherry or cotransfected with either GT-mCherry/GFP-AK1 or GT-mCherry/GFP-AK1B. Expression was allowed for 7 h, and then, cycloheximide was added. Cells were incubated with NZ for 3 h at 37°C and then for an additional 1 h on ice. Cells were rinsed with ice-cold medium, and warmed medium was added to induce MT regrowth. Transfected and cotransfected cells were identified and recorded at 30°C every 8 min for 7 h with an inverted microscope (DM16000; Leica) equipped with a camera (ORCA-ER; Hamamatsu Photonics) and using an HCX Plan Apochromat CS 63×/1.4 NA oil objective. Images were processed using the Leica software. Cells were finally fixed in 3% PFA, and the CTR position was determined by IF.

Migration and GA/CTR reorientation

For wound-healing assays, cells were plated onto Culture Insert over 35-mm glass-bottom dishes and grown in phenol red–free DME/F12. For GA/CTR reorientation assays, cells were fixed at 0, 3, 5, and 8 h after wounding. GA/CTR orientation was determined for the first row of cells. For cell migration experiments, images were captured at 10-min intervals for 24 h with an inverted microscope (DM16000) equipped with a camera (ORCA-ER) and using an N Plan Apochromat 10×/0.25 NA objective (Leica). Processing and analysis were performed using MetaMorph and Wimasis softwares. The CTR and GA were visualized using a 40× oil objective.

Primary cilium induction

For primary cilium induction experiments, RPE-1 cells grown on coverslips were either nontransfected or transfected with flag-AK1 or flag-AK1B constructions as described in Constructions, transfections, and RNAi interference. 6 h after transfection, cells were maintained with DME/F12 medium supplemented with 0.25% FBS, fixed with cold methanol at 0, 24, and 36 h after serum starvation, and processed for IF.

Online supplemental material

Fig. S1 shows subcellular localization of AKAP450-truncated mutants in RPE-1 and MCF10A cells. Fig. S2 shows the behavior of AK1 or AK1B fragments in RPE-1 cells treated with either NZ, taxol, or brefeldin A. Fig. S3 shows analysis of phenotypes induced by AK1 or AK1B fragment expression by using Y-shaped micropatterned coverslips. Fig. S4 shows that AKAP450 depletion induces the collapse of the GA around the CTR. Fig. S5 demonstrates that ERES redistribute with the GA in AK1- and AK1B-transfected cells. Video 1 shows live imaging of GA reassembly upon NZ washout in a GT-mCherry–transfected cell. Video 2 shows live imaging

of GA reassembly upon NZ washout in a GT-mCherry– and GFP-AK1–cotransfected RPE-1 cell. Video 3 shows live imaging of GA reassembly upon NZ washout in a GT-mCherry– and GFP-AK1B–cotransfected RPE-1 cell. Video 4 shows in vivo post-GA trafficking of Venus-NPY in polarized RPE-1 cells. Video 5 shows in vivo post-GA trafficking of Venus-NPY in polarized RPE-1 cells expressing the flag-AK1 construct. Video 6 shows in vivo post-GA trafficking of Venus-NPY in polarized RPE-1 cells expressing the flag-AK1B construct. Video 7 shows a wound-healing assay of control RPE-1 cells. Video 8 shows a wound-healing assay of GFP-AK1 RPE-1 transfected cells. Video 9 shows a wound-healing assay of GFP-AK1B RPE-1 transfected cells. Online supplemental material is available at http://www.jcb.org/cgi/content/full/jcb.201011014/DC1.

We thank Drs. Kaverina, Goud, Misumi, Malhotra, and Balch for providing reagents, Gergely for critical reading the manuscript, P. Dominguez for assistance in microscopy, and E. Garrido for IP.

Funding was provided by the Ministerio de Ciencia e Innovación (grants BFU2009-07182 and CSD2009-00016) and Junta de Andalucía (grant P07-CVI-03199) to R.M. Rios and C. Caballero. M.P. Gavilan is a Ministerio de Ciencia e Innovación–Juan de la Cierva fellow.

M. Bornens is acting as the chief scientific officer of the CYTOO company where micropatterns used in this work were purchased.

Submitted: 2 November 2010
Accepted: 29 April 2011

References

Barr, A.R., J.V. Kilmartin, and F. Gergely. 2010. CDK5RAP2 functions in centrosome to spindle pole attachment and DNA damage response. *J. Cell Biol.* 189:23–39. doi:10.1083/jcb.200912163

Bisel, B., Y. Wang, J.H. Wei, Y. Xiang, D. Tang, M. Miron-Mendoza, S. Yoshimura, N. Nakamura, and J. Seemann. 2008. ERK regulates Golgi and centrosome orientation towards the leading edge through GRASP65. *J. Cell Biol.* 182:837–843. doi:10.1083/jcb.200805045

Brownhill, K., L. Wood, and V. Allan. 2009. Molecular motors and the Golgi complex: staying put and moving through. *Semin. Cell Dev. Biol.* 20:784–792. doi:10.1016/j.semcdb.2009.03.019

Cardenas, J., S. Rivero, B. Goud, M. Bornens, and R.M. Rios. 2009. Golgi localisation of GMAP210 requires two distinct cis-membrane binding mechanisms. *BMC Biol.* 7:56. doi:10.1186/1741-7007-7-56

Chang, P., M. Coughlin, and T.J. Mitchison. 2005. Tankyrase-1 polymerization of poly(ADP-ribose) is required for spindle structure and function. *Nat. Cell Biol.* 7:1133–1139. doi:10.1038/ncb1322

Diao, A., D. Rahman, D.J. Pappin, J. Lucocq, and M. Lowe. 2003. The coiled-coil membrane protein golgin-84 is a novel rab effector required for Golgi ribbon formation. *J. Cell Biol.* 160:201–212. doi:10.1083/jcb.200207045

Efimov, A., A. Kharitonov, N. Efimova, J. Loncarek, P.M. Miller, N. Andreyeva, P. Gleeson, N. Galjart, A.R. Maia, I.X. McLeod, et al. 2007. Asymmetric CLASP-dependent nucleation of noncentrosomal microtubules at the trans-Golgi network. *Dev. Cell.* 12:917–930. doi:10.1016/j.devcel.2007.04.002

El Din El Homasany, B.S., Y. Volkov, M. Takahashi, Y. Ono, G. Keryer, A. Delouvée, E. Looby, A. Long, and D. Kelleher. 2005. The scaffolding protein CG-NAP/AKAP450 is a critical integrating component of the LFA-1-induced signaling complex in migratory T cells. *J. Immunol.* 175:7811–7818.

Follit, J.A., J.T. San Agustin, F. Xu, J.A. Jonassen, R. Samtani, C.W. Lo, and G.J. Pazour. 2008. The Golgin GMAP210/TRIP11 anchors IFT20 to the Golgi complex. *PLoS Genet.* 4:e1000315. doi:10.1371/journal.pgen.1000315

Gillingham, A.K., and S. Munro. 2000. The PACT domain, a conserved centrosomal targeting motif in the coiled-coil proteins AKAP450 and pericentrin. *EMBO Rep.* 1:524–529.

Hoppeler-Lebel, A., C. Celati, G. Bellett, M.M. Mogensen, L. Klein-Hitpass, M. Bornens, and A.M. Tassin. 2007. Centrosomal CAP350 protein stabilises microtubules associated with the Golgi complex. *J. Cell Sci.* 120:3299–3308. doi:10.1242/jcs.013102

Kardon, J.R., and R.D. Vale. 2009. Regulators of the cytoplasmic dynein motor. *Nat. Rev. Mol. Cell Biol.* 10:854–865. doi:10.1038/nrm2804

Kim, H.S., M. Takahashi, K. Matsuo, and Y. Ono. 2007. Recruitment of CG-NAP to the Golgi apparatus through interaction with dynein-dynactin complex. *Genes Cells*. 12:421–434. doi:10.1111/j.1365-2443.2007.01055.x

Kodani, A., and C. Sütterlin. 2008. The Golgi protein GM130 regulates centrosome morphology and function. *Mol. Biol. Cell*. 19:745–753. doi:10.1091/mbc.E07-08-0847

Kodani, A., I. Kristensen, L. Huang, and C. Sütterlin. 2009. GM130-dependent control of Cdc42 activity at the Golgi regulates centrosome organization. *Mol. Biol. Cell*. 20:1192–1200. doi:10.1091/mbc.E08-08-0834

Lam, C., M.A. Vergnolle, L. Thorpe, P.G. Woodman, and V.J. Allan. 2010. Functional interplay between LIS1, NDE1 and NDEL1 in dynein-dependent organelle positioning. *J. Cell Sci.* 123:202–212. doi:10.1242/jcs.059337

Liu, Y., M. Boukhelifa, E. Tribble, E. Morin-Kensicki, A. Uetrecht, J.E. Bear, and V.A. Bankaitis. 2008. The Sac1 phosphoinositide phosphatase regulates Golgi membrane morphology and mitotic spindle organization in mammals. *Mol. Biol. Cell*. 19:3080–3096. doi:10.1091/mbc.E07-12-1290

Miller, P.M., A.W. Folkmann, A.R. Maia, N. Efimova, A. Efimov, and I. Kaverina. 2009. Golgi-derived CLASP-dependent microtubules control Golgi organization and polarized trafficking in motile cells. *Nat. Cell Biol.* 11:1069–1080. doi:10.1038/ncb1920

Pitaval, A., Q. Tseng, M. Bornens, and M. Théry. 2010. Cell shape and contractility regulate ciliogenesis in cell cycle–arrested cells. *J. Cell Biol.* 191:303–312. doi:10.1083/jcb.201004003

Prigozhina, N.L., and C.M. Waterman-Storer. 2004. Protein kinase D-mediated anterograde membrane trafficking is required for fibroblast motility. *Curr. Biol.* 14:88–98. doi:10.1016/j.cub.2004.01.003

Puthenveedu, M.A., C. Bachert, S. Puri, F. Lanni, and A.D. Linstedt. 2006. GM130 and GRASP65-dependent lateral cisternal fusion allows uniform Golgi-enzyme distribution. *Nat. Cell Biol.* 8:238–248. doi:10.1038/ncb1366

Rios, R.M., A. Sanchís, A.M. Tassin, C. Fedriani, and M. Bornens. 2004. GMAP-210 recruits gamma-tubulin complexes to cis-Golgi membranes and is required for Golgi ribbon formation. *Cell*. 118:323–335. doi:10.1016/j.cell.2004.07.012

Rivero, S., J. Cardenas, M. Bornens, and R.M. Rios. 2009. Microtubule nucleation at the cis-side of the Golgi apparatus requires AKAP450 and GM130. *EMBO J.* 28:1016–1028. doi:10.1038/emboj.2009.47

Robles-Valero, J., N.B. Martín-Cófreces, A. Lamana, S. Macdonald, Y. Volkov, and F. Sánchez-Madrid. 2010. Integrin and CD3/TCR activation are regulated by the scaffold protein AKAP450. *Blood*. 115:4174–4184. doi:10.1182/blood-2009-12-256222

Satir, P., L.B. Pedersen, and S.T. Christensen. 2010. The primary cilium at a glance. *J. Cell Sci.* 123:499–503. doi:10.1242/jcs.050377

Sehrawat, S., T. Ernandez, X. Cullere, M. Takahashi, Y. Ono, Y. Komarova, and T.N. Mayadas. 2011. AKAP9 regulation of microtubule dynamics promotes Epac1-induced endothelial barrier properties. *Blood*. 117:708–718. doi:10.1182/blood-2010-02-268870

Sengupta, D., S. Truschel, C. Bachert, and A.D. Linstedt. 2009. Organelle tethering by a homotypic PDZ interaction underlies formation of the Golgi membrane network. *J. Cell Biol.* 186:41–55. doi:10.1083/jcb.200902110

Steinmetz, M.O., and A. Akhmanova. 2008. Capturing protein tails by CAP-Gly domains. *Trends Biochem. Sci.* 33:535–545. doi:10.1016/j.tibs.2008.08.006

Sütterlin, C., and A. Colanzi. 2010. The Golgi and the centrosome: building a functional partnership. *J. Cell Biol.* 188:621–628. doi:10.1083/jcb.200910001

Sütterlin, C., P. Hsu, A. Mallabiabarrena, and V. Malhotra. 2002. Fragmentation and dispersal of the pericentriolar Golgi complex is required for entry into mitosis in mammalian cells. *Cell*. 109:359–369. doi:10.1016/S0092-8674(02)00720-1

Sütterlin, C., R. Polishchuk, M. Pecot, and V. Malhotra. 2005. The Golgi-associated protein GRASP65 regulates spindle dynamics and is essential for cell division. *Mol. Biol. Cell*. 16:3211–3222. doi:10.1091/mbc.E04-12-1065

Takahashi, M., H. Shibata, M. Shimakawa, M. Miyamoto, H. Mukai, and Y. Ono. 1999. Characterization of a novel giant scaffolding protein, CG-NAP, that anchors multiple signaling enzymes to centrosome and the golgi apparatus. *J. Biol. Chem.* 274:17267–17274. doi:10.1074/jbc.274.24.17267

Takahashi, M., A. Yamagiwa, T. Nishimura, H. Mukai, and Y. Ono. 2002. Centrosomal proteins CG-NAP and kendrin provide microtubule nucleation sites by anchoring gamma-tubulin ring complex. *Mol. Biol. Cell*. 13:3235–3245. doi:10.1091/mbc.E02-02-0112

Thyberg, J., and S. Moskalewski. 1999. Role of microtubules in the organization of the Golgi complex. *Exp. Cell Res.* 246:263–279. doi:10.1006/excr.1998.4326

Vinogradova, T., P.M. Miller, and I. Kaverina. 2009. Microtubule network asymmetry in motile cells: role of Golgi-derived array. *Cell Cycle*. 8:2168–2174. doi:10.4161/cc.8.14.9074

Wolff, A., B. de Néchaud, D. Chillet, H. Mazarguil, E. Desbruyères, S. Audebert, B. Eddé, F. Gros, and P. Denoulet. 1992. Distribution of glutamylated alpha and beta-tubulin in mouse tissues using a specific monoclonal antibody, GT335. *Eur. J. Cell Biol.* 59:425–432.

Yadav, S., S. Puri, and A.D. Linstedt. 2009. A primary role for Golgi positioning in directed secretion, cell polarity, and wound healing. *Mol. Biol. Cell*. 20:1728–1736. doi:10.1091/mbc.E08-10-1077